Nonlinear Identification of Transient Tank Vertical Sloshing Motions

L. Constantin [1], J. de Courcy [1] B. Titurus [1], T. Rendall [1] , J.E. Cooper [1]

[1] Dept of Aerospace Engineering, University of Bristol
Queens Building, University Walk, Bristol, BS8 1TR, UK

e-mail: **j.e.cooper@bristol.ac.uk**

Abstract

In an effort to reduce the fuel burn of commercial jet aircraft, much effort is currently being devoted towards reducing the loads that aircraft experience in-flight due to gusts and turbulence using a range of passive and active methodologies. The EU H2020 SLOW-D project is undertaking a series of fundamental experiments to gain an understanding of vertical sloshing and the added damping that these motions provide, and to apply them for future aircraft wing designs. Recent transient and harmonic experiments undertaken as part of SLOW-D have shown that the added damping from the vertical sloshing motion is a function of the motion amplitude, filling level and excitation frequency. Further, the transient tests have shown that the added damping to a single DOF system comprises three different physical sloshing regimes, whereas the harmonic tests show the importance of the Froude number. In this paper, a selection of the experimental transient data sets from vertical sloshing experiments are analysed using nonlinear identification techniques based upon NAR and NARX models. It is shown how a continuous time model can be identified that accurately predicts the variation of the damping with amplitude and frequency. Surrogate models of identified parameters are developed to enable parametric studies.

1 Introduction

There is a continuing drive to reduce the environmental impact of civil jet aircraft, partly by improving performance through a decrease in fuel burn. This important goal can only be achieved through improving specific fuel consumption, the lift to drag ratio, flight/ground operations or reducing aircraft weight. All aircraft are subject to a range of different loads during flight and ground operations and these lead to the critical design cases which define the sizing, and hence the weight, of the aircraft structure. One approach to achieve weight reduction is through the use of loads alleviation concepts to reduce the effect of turbulence, gusts and flight manoeuvres. Many different types of active and passive approaches have been used to achieve loads alleviation, including the conventional aerodynamic approach using control surfaces or spoilers whose motion is defined by an active control law related to the motion of the aircraft. Passive structural concepts are feasible but not yet widely implemented, including aeroelastic tailoring to couple the wing bending / torsion motions in a beneficial manner and also the use of folding wingtips.

In the civil engineering field there have been many cases of using some form of fluid in a tank as a tuned liquid damper (TLD) to reduce the lateral response of tall buildings to the wind or earthquakes. Tuned mass dampers (TMD) are relatively common in civil aircraft being used for instance to reduce the vibration and noise associated with engines or aeroelastic response. However, they tend to consist of mechanical systems rather than sloshing of a fluid in a tank, and have not been applied to gust or turbulence loads. With regard to damping in vertical vibratory systems, extensive work has been carried out on particle impact damping, where energy is dissipated through momentum exchange between particles of different sizes and the structure. Vertically-excited systems containing liquids have also been studied previously, with applications

such as liquid propellant tanks or water towers. Relatively little work has considered such an approach for civil aircraft, with preliminary studies focused on numerical investigations on integration of fuel sloshing in aeroelastic models.

SLOWD (Sloshing Wing Dynamics) is an Airbus-led EU H2020 funded project that commenced in September 2019 to investigate the use of sloshing in aircraft wing fuel tanks to reduce the loading effects of gusts and turbulence. The project is aimed at developing fluid-structure interaction technologies to enhance the design of fuel tanks and their use such that loads reduction is achieved, leading to improved fuel efficiency and reduced environmental impact through structural weight savings. As part of this effort, some preliminary tests considered a cantilevered beam with attached water tanks subjected to vertical step-release transient excitation [1]. It was found that the addition of the liquid increased the damping in the transient response, and that this damping was dependent upon the amount of liquid in the tanks. Although a good example of the possibility of exploiting fuel sloshing motion to impart added damping to aircraft wing motion, it was a difficult set-up for comparing the various fluid sloshing modelling capabilities being developed in the SLOWD project.

Recent transient [2] and harmonic excitation [3] experiments undertaken as part of SLOW-D have shown that the added damping from the sloshing motion is a function of forcing amplitude, frequency and fuel level [4]. The transient tests have showed that the added damping to a single DOF system comprises of three different physical sloshing regimes that are function of the amplitude, whereas the harmonic tests show the importance of the Froude number, defined as the square root of the ratio of the inertial to gravitational forces and formulated as the ratio of peak displacement A times the angular frequency over gravity such that

$$Fr = \sqrt{\frac{A\omega^2}{g}} \tag{1}$$

Previous identification studies on the transient data have used a linear piece-wise identification approach to identify three separate damping values [1] [2].

In this paper, the experimental transient and harmonic data sets are analysed using a number of nonlinear identification techniques based upon NAR and NARX models [5]. It is shown how a continuous time model can be estimated that accurately predicts the variation of the damping with amplitude and frequency. Surrogate models of identified parameters are developed to enable parametric studies of the effects of amplitude, fill level, frequencies, etc.

2 Overview of 1DOF Vertical Sloshing Tests

2.1 Experimental Set-Up

Transient tests were undertaken using a T-Beam flexure type configuration manufactured from two perpendicular steel strips, (1) in Figure 1, with its three ends constrained [2] [4]. A tank (2) (height h = 20 mm, length L = 60 mm and width w = 30mm) was placed in the middle of the horizontal beam alongside an additional mass (3) to maintain dynamic equivalence between tests at various filling levels. The system was loaded vertically using a turnbuckle (5) and released by cutting the wire, and the response of the system was measured using an accelerometer (4) placed under the tank. This experimental arrangement showed only one dominant lightly damped vibration mode with a linear domain extending up to at least 14 strip thicknesses. These properties made the chosen configuration ideal for vertical transient sloshing studies. The amplitudes of excitation studied here are in the range of 1 – 14mm and filling levels between 0 and 100% with increments of 10% are considered as well.

The harmonic experiments [3] [4] employed a linear actuator to impose a controlled vertical sinusoidal motion on the sloshing tank. The experimental setup, see Figure 2, consisted of a vertical actuator capable of large amplitudes of motion (either electromechanical actuator or long-stroke electrodynamic shaker) grounded on a vibration isolation table. Two actuators were used in order to expand the test matrix, as the

electromechanical actuator was found to be limited in the achievable accelerations and also presented more mechanical noise. Two tanks partially filled with liquid (tank 1: h = 37.5mm, L = 100mm, w = 30mm; tank 2: h = 50mm, L = 100mm, w = 30mm) were placed at the end of the actuator with an accelerometer and force sensor in between. Two tanks were used in order to investigate the influence of tank height. Considering that the tests were conducted separately at set amplitude and frequency, the tank acceleration information obtained from one single accelerometer was sufficient to completely describe, using suitable processing of the data, the displacement, velocity and acceleration of the tank. The force sensor placed between the actuator and the tank was used to isolate the force due to the moving liquid. This force was then integrated with respect to tank displacement and normalized to obtain a measure of non-dimensional energy dissipation.

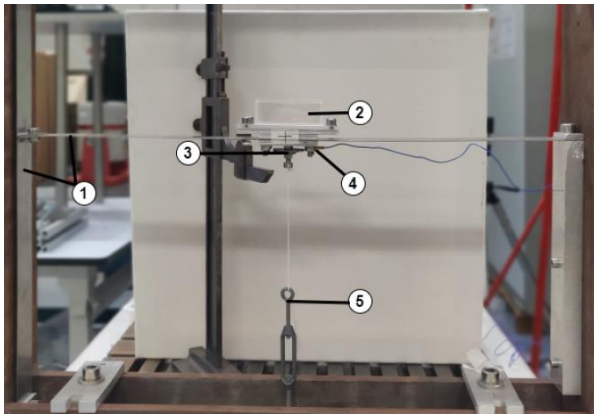

Figure 1. T-Beam Transient Test

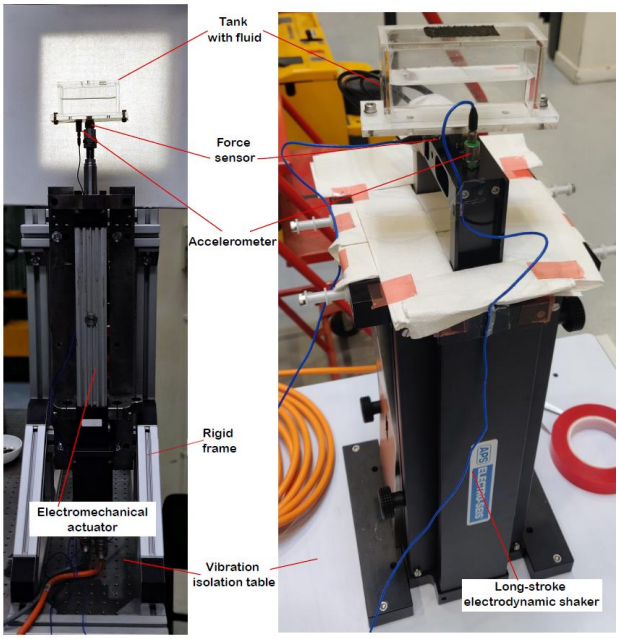

Figure 2. Prescribed Harmonic Motion Set-Up

2.2 Typical Test Results

2.2.1 Transient Tests

Transient tests were conducted with various initial amplitudes and filling levels. Figure 3 shows a typical sloshing tank acceleration time response, with black curves indicating mean decay data at each time instant, and the red bands showing the minimum / maximum confidence bounds from three repeated tests. The results shown here are for the 50% filling level. Fig 3a contains insets showing the single frequency dominance in the system, as well as the measure variability in the data and how it changes with time. Very good repeatability is observed. Figure 3b shows the envelopes of the same acceleration decays on a semi-logarithmic scale, with the damping ratio ξ computed from the slope of the envelope and expressed as percentage of critical damping. The trends corresponding to the dry structure are also shown and the marked difference through the addition of liquid can be seen. Of particular note is the piecewise linear nature of the envelope on the semi-logarithmic plots, indicative of separate damping trends. These regions are referred to as R1 – R3 and representative video captures are seen in Figure 4. The different sloshing behaviour corresponds to distinct damping levels defined as:

- R1 – the most dissipative region is dominated by violent vertical liquid impacts with the top and bottom of the tank
- R2 – substantial energy dissipation caused by lower amplitude sloshing motions dominated by one or multiple liquid sloshing modes (mode (2,0) in the case shown in Figure 8) also known as Faraday waves
- R3 - low amplitude surface ripples or no liquid movement at all, where the energy dissipation is the same as the low-amplitude dry structure response.

The behaviour of the single degree of freedom transient systems were found to be highly dependent on amplitude of excitation and filling level. Tests were conducted for filling levels starting from 0 to 100%, with increments of 10%, and a summary of all identified damping trends for the maximum excitation amplitude are shown in Figure 5 for each of the three sloshing regions. Both the 0% and 100% cases show zero sloshing-induced dissipation, as there is no liquid or it does not move. Between the two extremes, the R1 damping ratio was found to increase until 50% filling level and then to decrease back. There is substantial symmetry in effective about the 50% filling level. The R2 damping ratio was found to be less dependent on filling level, since damping in this region is dominated by certain liquid sloshing patterns in which filling level plays only a limited role (frequency of excitation is the most important parameter here). Understanding the variation of damping to due vertical sloshing with respect to filling ratio is of utmost importance in exploiting the liquid sloshing action in order to maximize the induced damping effects.

Finally, a global view of the R1 sloshing-induced dissipation trends can be seen in Figure 6 for three filling levels and initial excitation amplitudes up to 7.5g. Each marker is a single experimental data point corresponding to $\zeta 1$ in the R1 region, and two straight lines were fitted in order to show the damping trends. The damping ratio is seen to increase in value up to between 3 and 4g, after which a plateau is reached with a slightly increasing trend. Further work [4] has shown that with a further increase in maximum acceleration level the R1 damping level starts to decrease.

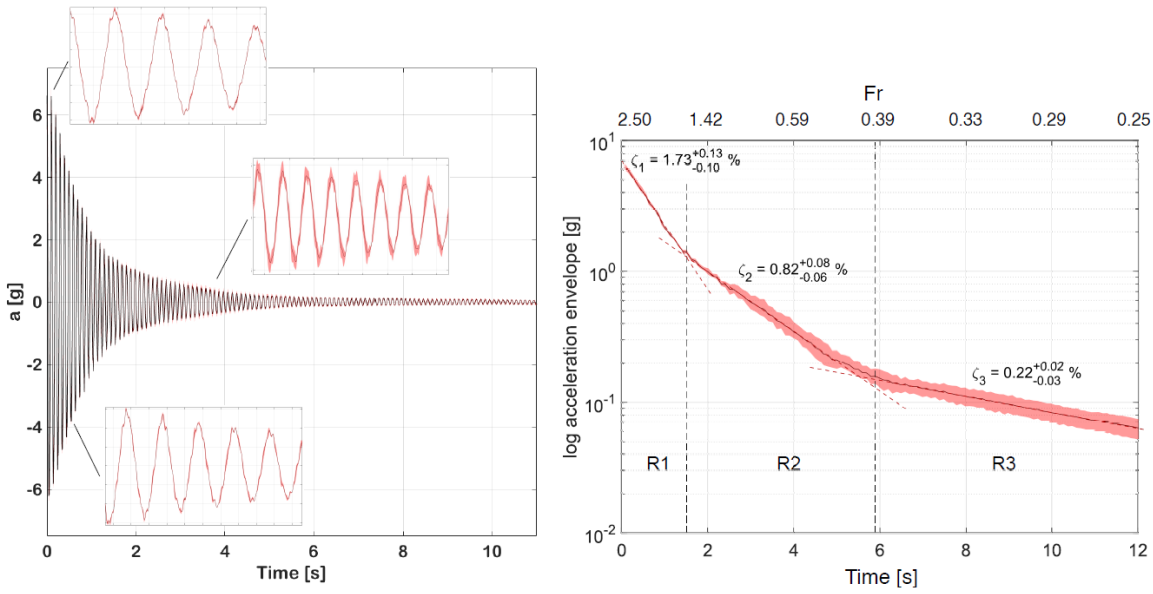

Figure 3. Typical Transient Response - a. Time History and b. Envelopes [4]

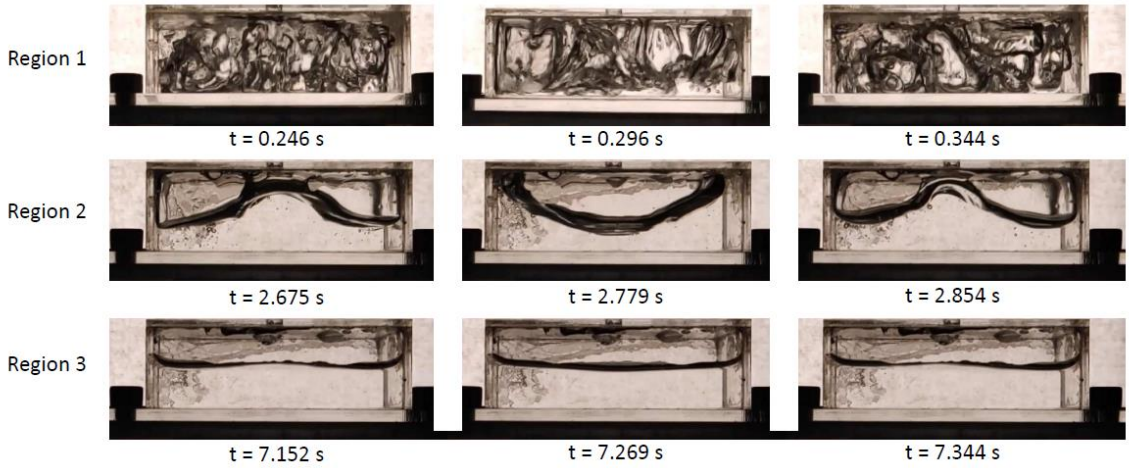

Figure 4. Different Sloshing Regimes During Transient Tests [4]

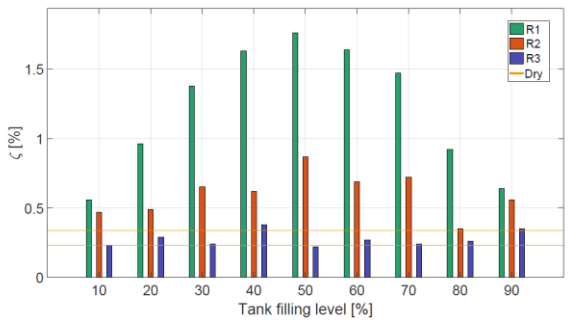

Figure 5. Damping for Different Regions and Tank Filling Levels [4]

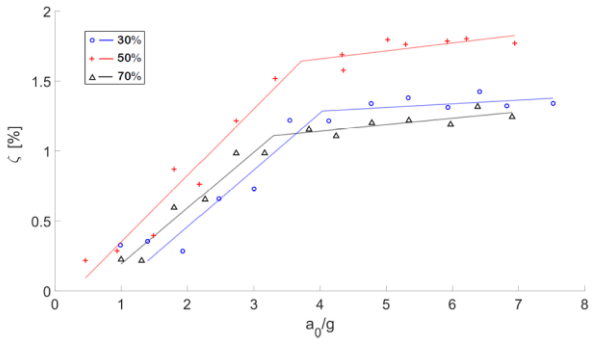

Figure 6. R1 Damping Level versus Maximum Acceleration [4]

2.2.2 Harmonic Tests

Only the 50% fill case is considered for harmonic tests.Through excitation at a single frequency, it is possible to excite sloshing regions R1 and R2, and it was found that there is also a mixed mode case which combines the R1 and R2 motions. Figure 7 shows video snapshots of these motions and these are shown in some detail in Figure 8 where an average of the wave fronts are shown from 25 completed cycles for increasing Froude number Fr. Between $0.67 \le Fr \le 1.07$ the lateral fluid sloshing motion is clearly seen, for $1.17 \le Fr \le 1.44$ the mixed mode occurs with the lateral motion combining with occasion contacts with the upper tank surface, and finally for $1.52 \le Fr \le 1.80$ the violent chaotic sloshing motion occurs with hits on both the upper and lower surfaces.

The dissipative energy due to sloshing, obtained from the force and resulting tank motion [3] [4], leads to the results shown in Figure 9 where, as for the transient case, there is a much greater energy dissipation from the R1 motion compared to R2. In the combined R1 & R2 region the energy dissipation varies in a linear manner with increasing Froude number.

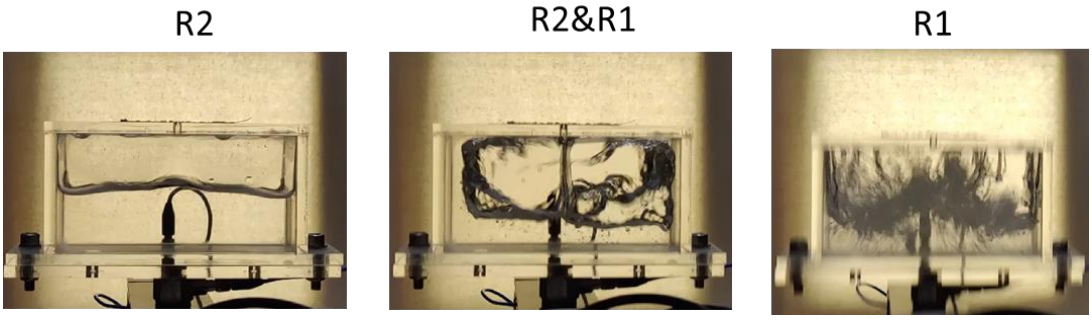

Figure 7. Different Sloshing regimes Excited During Harmonic Tests [4]

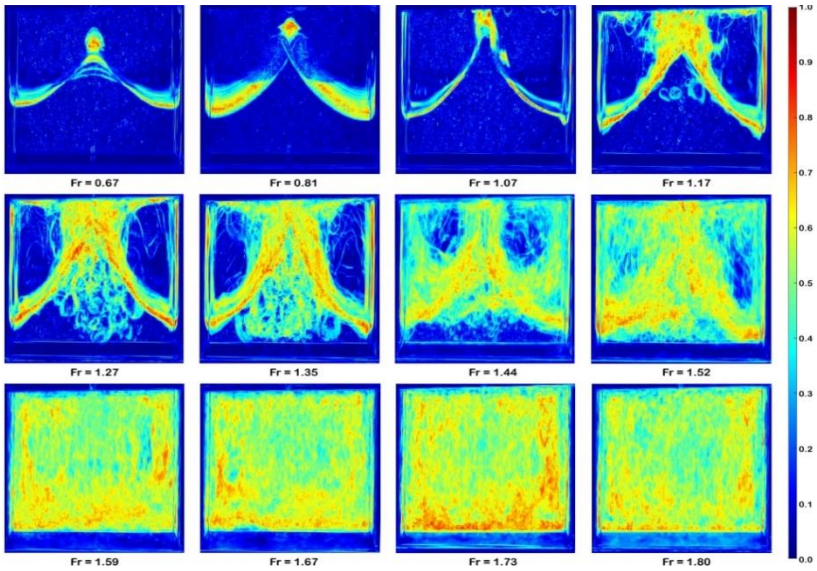

Figure 8. Averaged Results from 25 Cycles [4]

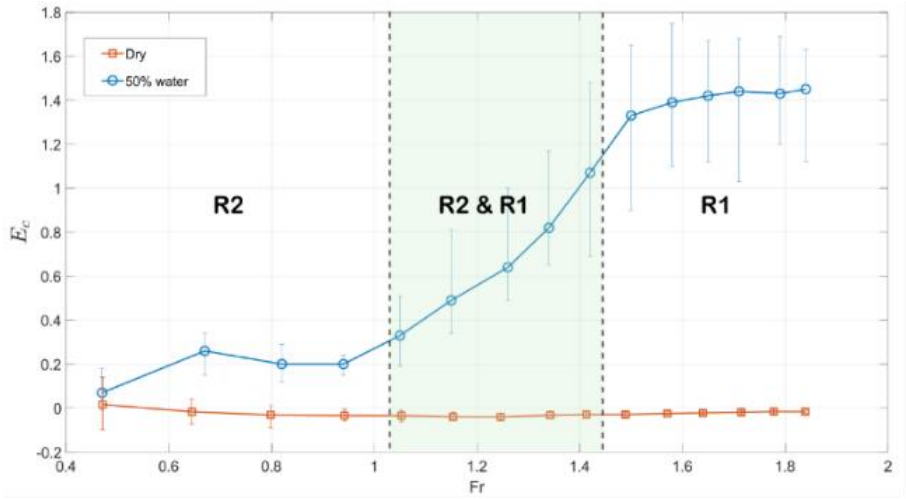

Figure 9. Energy Extracted For Different Harmonic Excitation Frequencies [4]

3 Mathematical Modelling

It is well known that for a linear time invariant M DOF system undergoing a transient response can be represented as an Autoregressive (AR) equation such that

$$y_j + a_1 y_{j-1} + a_2 y_{j-2} + \quad \ldots \quad + a_{2M} y_{j-2M} = \varepsilon_j \tag{2}$$

where y_k represents the measured output at time instance $k\Delta t$ for a single physical measurement station and ε_k is the error (or residual) on the signal due to measurement noise or imperfections in the system. The a_k parameters are the unknowns that have to be estimated in the system identification process, and once this is achieved, the roots of the corresponding characteristic equation

$$\lambda^{2M} + a_1 \lambda^{2M-1} + a_2 \lambda^{2M-2} + \quad \ldots \quad + a_{2M} = 0 \tag{3}$$

lead, for oscillatory modes, to complex conjugate pairs in the form

$$\lambda = e^{\left(-\xi\omega \pm j\omega\sqrt{1-\xi^2}\right)\Delta t} \tag{4}$$

and hence the system natural frequencies ω and damping ratios ξ can be determined from

$$\begin{aligned}
&\lambda = \lambda_{\mathrm{R}} + \mathrm{i}\lambda_{\mathrm{I}} = \mathrm{e}^{\left(-\xi\omega \pm \mathrm{i}\omega\sqrt{1-\xi^2}\right)\Delta \mathrm{t}} \\
&\rightarrow \ln\left(\lambda_{\mathrm{R}} + \mathrm{i}\lambda_{\mathrm{I}}\right) = \ln\left(\sqrt{\lambda_{\mathrm{R}}^2 + \lambda_{\mathrm{I}}^2}\right) + \mathrm{i}\tan^{-1}\left(\frac{\lambda_{\mathrm{I}}}{\lambda_{\mathrm{R}}}\right) = \mathrm{p} + \mathrm{iq} = \left(-\xi\omega \pm \mathrm{i}\omega\sqrt{1-\xi^2}\right)\Delta \mathrm{t} \\
&\rightarrow \mathrm{p} = -\xi\omega\Delta \mathrm{t} \qquad \mathrm{q} = \omega\sqrt{1-\xi^2}\,\Delta \mathrm{t} \\
&\rightarrow \omega = \frac{\sqrt{\mathrm{p}^2 + \mathrm{q}^2}}{\Delta \mathrm{t}} \quad \text{and} \quad \xi = \frac{-\mathrm{p}}{\sqrt{\mathrm{p}^2 + \mathrm{q}^2}}
\end{aligned} \tag{5}$$

Note that due to the difference equation nature of the AR model (a dependency upon previous time values) a simple least squares identification process is likely to produce very biased estimates unless model order overspecification is employed, such as in the LSCE, ERA and Polymax identification methods.

If there is an measured input u_k to the system, then the AR model extends to an ARMAX model in the form

$$y_j + a_1 y_{j-1} + a_2 y_{j-2} + \quad \ldots \quad + a_{2M} y_{j-2M} + p_1 u_{j-1} + p_2 u_{j-2} + \quad \ldots \quad + p_{2M} u_{j-2M} = \varepsilon_j \tag{6}$$

and the identification process is now required to find the unknown a_k and p_k parameters.

The addition of nonlinear terms, as introduced in the classic NARMAX method [5], is well documented. Here we briefly show that a 1DOF NAR (nonlinear autoregressive) model with quadratic and cubic terms then equation (2) can be written as

$$\begin{aligned}
&y_j + a_1 y_{j-1} + a_2 y_{j-2} \\
&\quad + b_1 y_{1\,j-1}^2 + b_2 y_{j-1} y_{j-2} + b_3 y_{j-2}^2 \\
&\quad + c_1 y_{1\,j-1}^3 + c_2 y_{j-1}^2 y_{j-2} + c_3 y_{j-1} y_{j-2}^2 + c_4 y_{j-2}^3 = \varepsilon_j
\end{aligned} \tag{7}$$

and so on for higher order nonlinear terms. The number of unknown parameters can rapidly increase, particularly if a MDOF system is being considered, but the sloshing experiments discussed above are all single DOF. A similar approach can be used for the NARMAX models.

4 Transient Sloshing Identification

The transient responses were identified using the approach of rewriting equations (2) and (7) for different time instances and this can then be put into the well-known matrix formulation

$$\underline{y} = \phi\underline{\theta} + \underline{\varepsilon} \tag{8}$$

The classical Least Squares solution for the AR and NAR parameters $\underline{\theta}$ is found as

$$\underline{\theta} = \left(\phi^{T}\phi\right)^{-1}\phi^{T}\underline{y} \tag{9}$$

however, without model order overspecification there is likely to be biased. Consequently, an Instrumental Variables approach has been employed [6] here such that

$$\underline{\theta} = \left(\psi^{T}\phi\right)^{-1}\psi^{T}\underline{y} \tag{10}$$

where the "instruments" making up matrix ψ are found from delayed observations of the ϕ matrix.

4.1 50% fill level

Consider the transient response, and corresponding decay envelope shown in Figure 10 for the 50% filling level case. Initially the R1 and R2 regions were considered separately and identification performed using Log Decrement and the LS and IV approaches using the correct model order (2). It can be seen in Figure 11 how there are significant differences in the regenerated LS transient decays, indicating biased results; however, with an appropriate time delay there is a much better correspondence for the IV estimates, indicating that any bias can be eliminated.

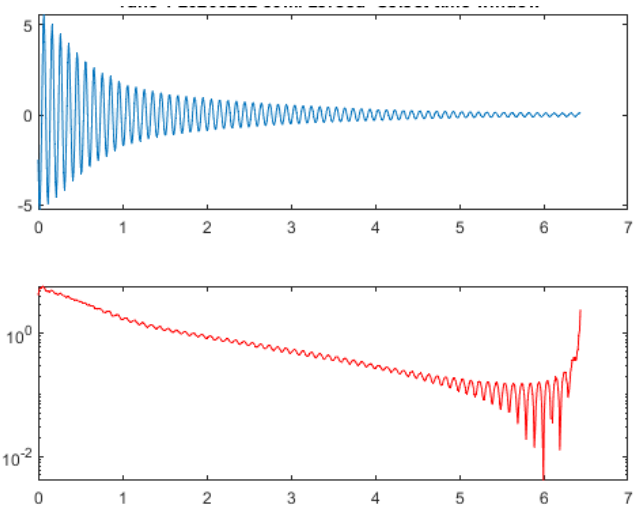

Figure 10. 50% Fill. Time History and Envelope

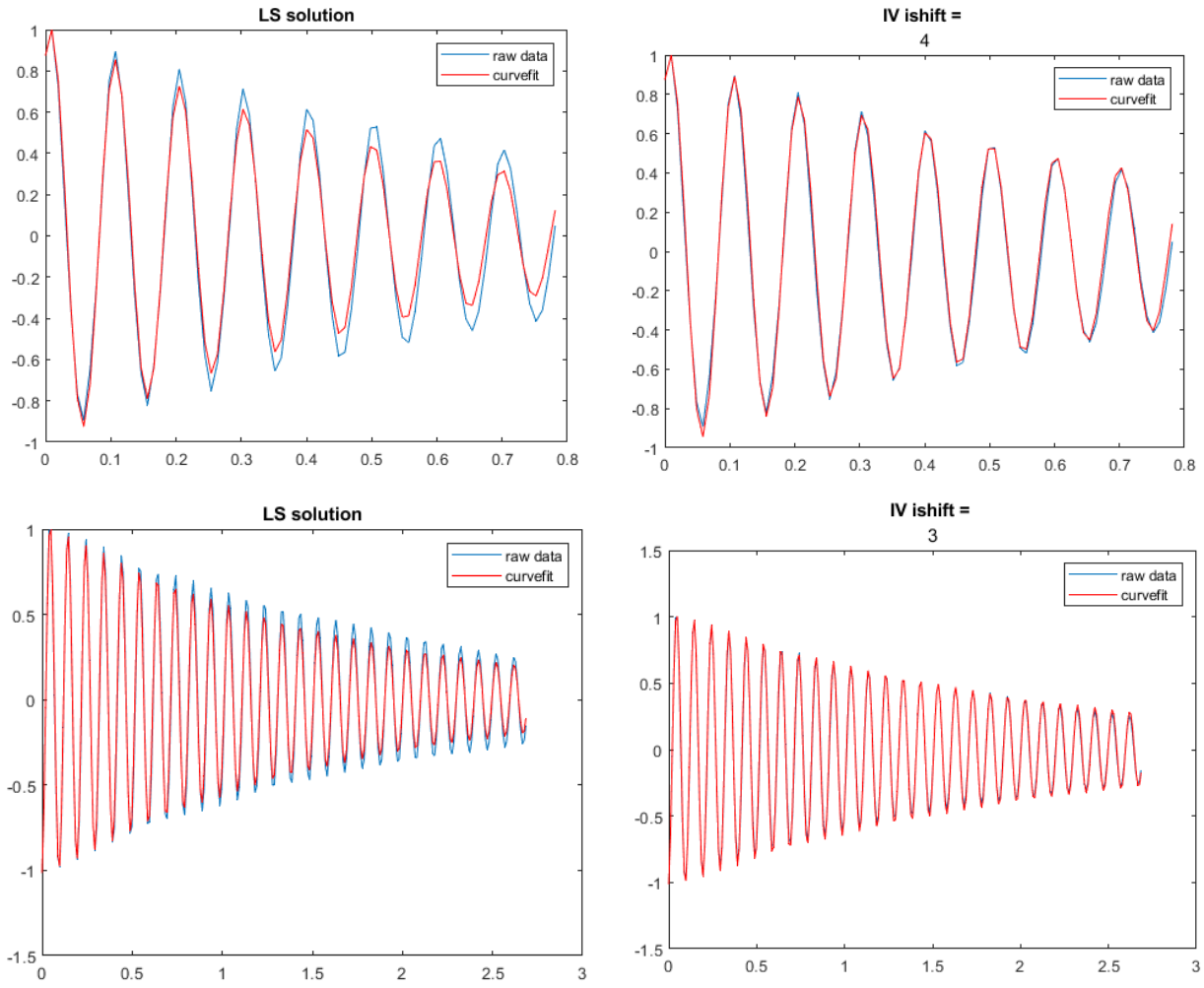

Figure 11. Linear Curve-fits of R1(left) and R2 (right) Regions. Least Squares and IV Approaches

The next part of the analysis consisted of identifying the R1 and R2 regions together which includes the piece-wise step in damping between the two sections. Table 1 shows some of the computed results for different terms included in equation (7) with the error function being defined as a function of the experimental data y_j and the regenerated data y_j^{est} such that

$$\varepsilon = \frac{\sum_{j=1}^{npts}\left(y_j - y_j^{est}\right)^2}{npts} \tag{11}$$

Table 1 and Figure 12 show the fitting error for a range of different orders of nonlinearity, note that all possible combinations of a particular order have been included whereas a full investigation should include the consideration of the contribution made by each individual term. It can be seen that there is a steady improvement in the LS curve-fits as the number of terms increases, particularly once the cubic terms are added. For the IV models there is little improvement beyond the addition of cubic terms, indeed in some cases the estimates get slightly worse. Figures 13 – 15 show typical curve-fits for different numbers of nonlinear terms, in all cases the IV fits are better.

Table 1. Fitting Error for Different Nonlinear Terms Included in the Mathematical Model

Model Used	**No of terms**	**Least Squares**	**Instrumental Variables**
linear	2	0.0065332	0.0016419
linear + quad	2+3	0.003862	0.0019715
linear + cubic	2+4	0.0057637	0.0010561
linear + quad + cubic	2+3+4	0.0023476	0.0010486
linear + quartic	2+5	0.0014893	0.0010388
linear + quintic	2+6	0.0042311	0.0020464
linear + cubic + quintic	2+4+6	0.0033849	0.0013243
linear + cubic + quartic	2+4+5	0.0012651	0.0012326
linear + quad + quartic	2+3+5	0.0018609	0.0011981
linear + quad + cubic + quartic	2+3+4+5	0.00088653	0.00095246

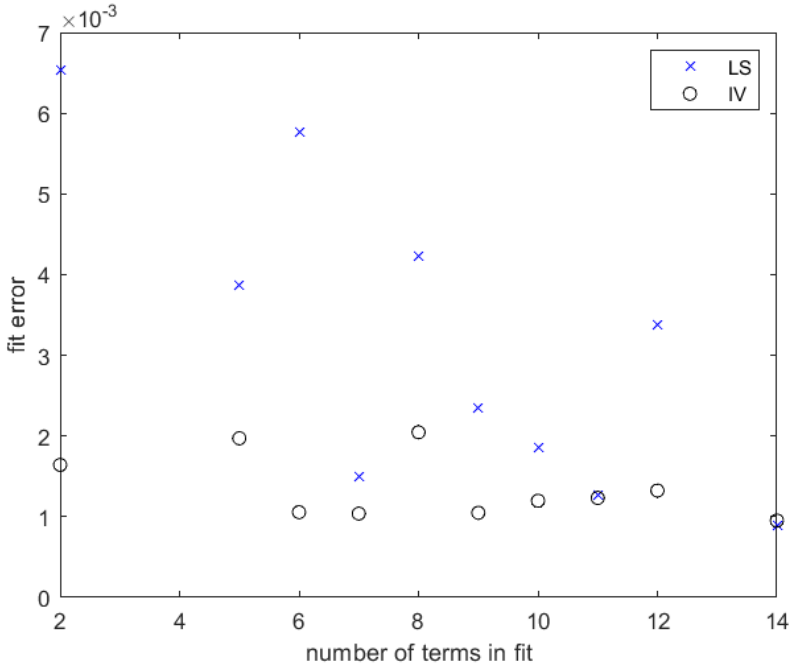

Figure 12. Fit Error vs Number of Parameters in the Mathematical Model

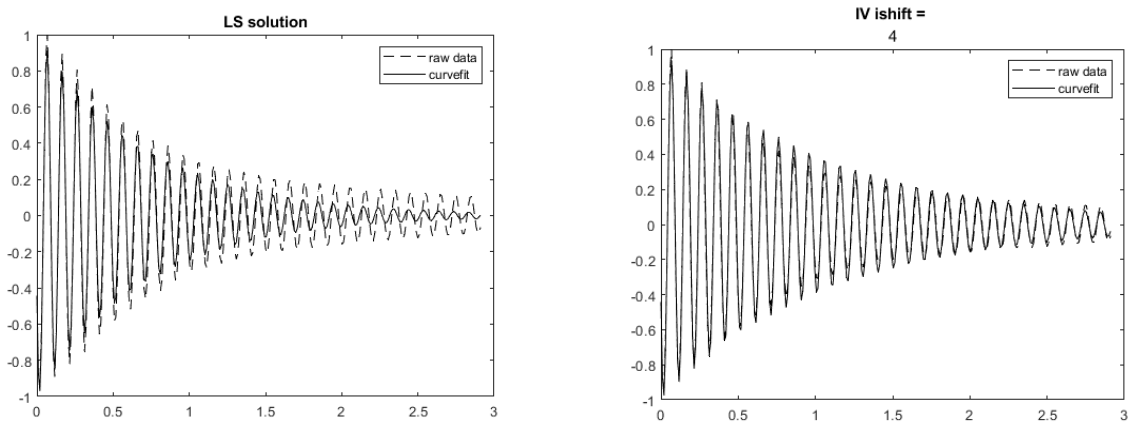

Figure 13. Linear Curve-fits of both Regions. Least Squares and IV Approaches

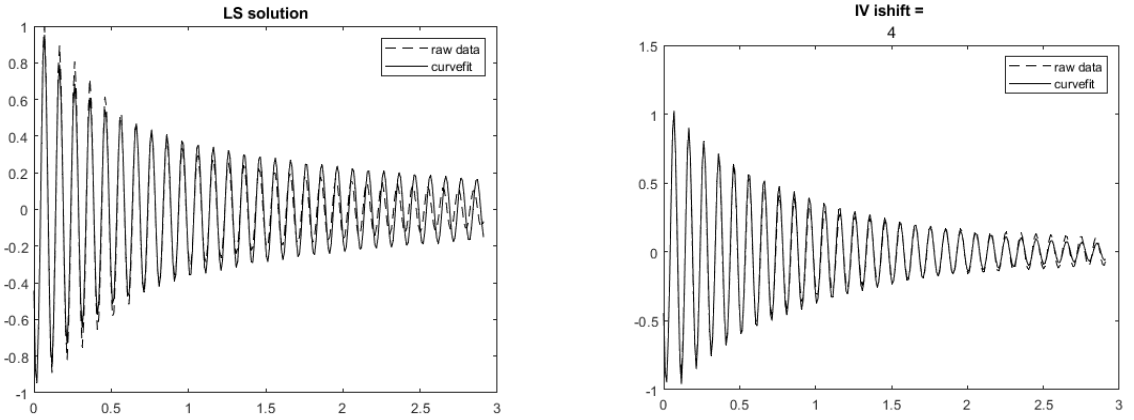

Figure 14. Linear + Cubic Curve-fits of both Regions. Least Squares and IV Approaches

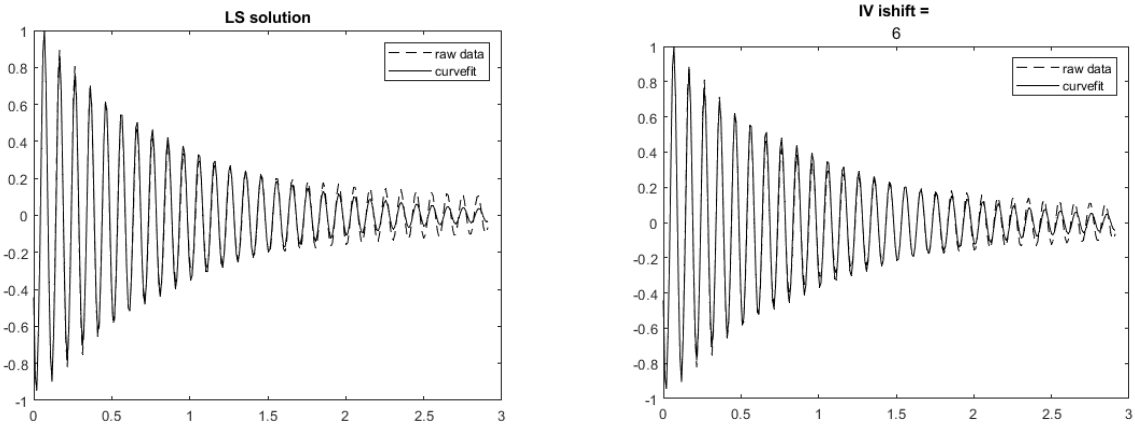

Figure 15. Linear + Cubic + Quintic Curve-fits of both Regions. Least Squares and IV Approaches

4.2 Varying the Fill Level

Having determined that an IV identification performed using linear and cubic terms (i.e. a_i and c_i terms in equation (7)) gave good results for the 50% filling case, the same model was applied to the R1 and R2 ranges for transient decays from 10% filling level through to the 90% level. Envelopes of all these transient responses are shown in Figure 16 and it can be seen that there is more of a dog-leg for the cases where there is more damping (not easily distinguished by eye as the time window is different for each case). Note that an additional mass was added or removed depending so that the total weight of the fluid and added mass was the same for all filling levels.

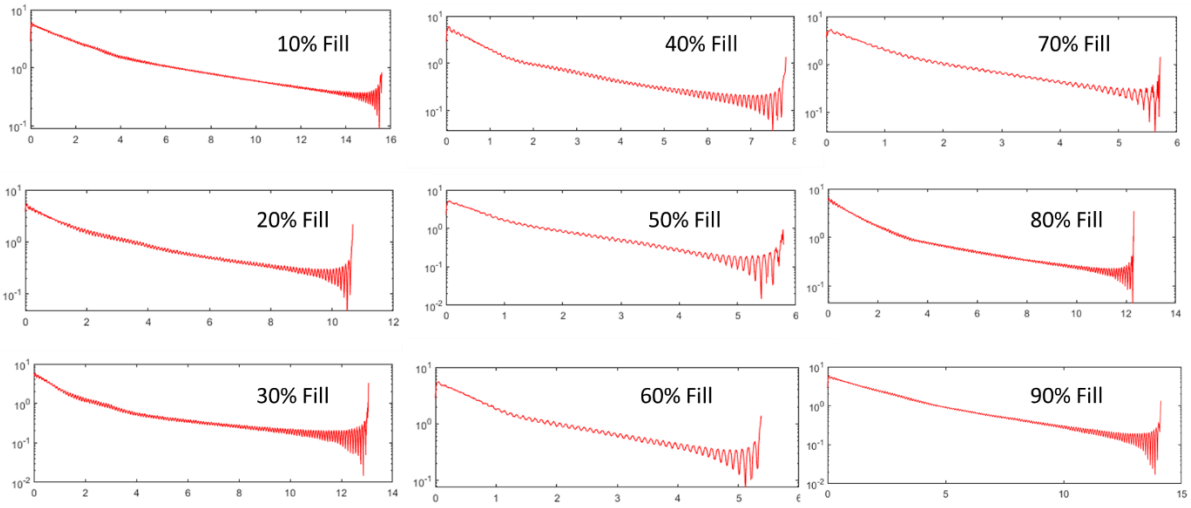

Figure 16. Transient Envelopes for Different Fill Levels

Table 2. Estimated IV Linear and Cubic Parameters for Different Filling Levels

Fill level(%)	a1	a2	c1	c2	c3	c4	Linear Frq (Hz)	Linear Damp(%)
10	1.6283	-0.9917	0.0993	-0.0903	-0.1809	0.1245	9.9661	0.68
20	1.6307	-0.9939	0.4631	-1.5355	1.0620	-0.0760	9.9576	0.50
30	1.6104	-0.9757	0.2442	-0.9312	0.8080	-0.1396	10.0350	1.99
40	1.6154	-0.9819	0.3666	-1.4096	1.2080	-0.1946	10.0356	1.48
50	1.6176	-0.9824	0.1972	-0.9822	0.9724	-0.1961	10.0102	1.44
60	1.6214	-0.9851	0.1434	-0.6320	0.5576	-0.0922	9.9876	1.22
70	1.6177	-0.9845	0.2395	-0.9477	0.8303	-0.1326	10.0330	1.26
80	1.6255	-0.9880	0.1366	-0.4224	0.2470	0.0024	9.9630	0.98
90	1.6281	-0.9929	-0.0414	0.0640	-0.0103	-0.0098	9.9828	0.58

Table 2. and Figure 17. show the identified parameters for the a_i (linear) and c_i (cubic) models that were identified and also the underlying natural frequencies and damping ratios from the linear part of the model. Curve-fits of similar quality to the 50% case shown above. There is very little variation in the linear parameters; however, as seen in Figure 17, although there is little change for the natural frequency, the

damping values does show more deviation, a function of the sensitivity of the damping to the a_2 coefficient, a behaviour also shown in Figure 18.

There is much more change in the nonlinear parameters particularly the c_2 and c_3 coefficients, with a larger variation around the middle fill levels, corresponding to a larger variation between the R1 and R2 regions. Towards the edges of the fill range, where the damping difference is much less, the magnitude of the cubic terms becomes almost zero. The underlying linear damping shown in Figure 18 is greater than the R3 values seen in Figure 5 but this can be explained by the fact that the analysis undertaken here has only considered the R1 and R2 parts of the decay.

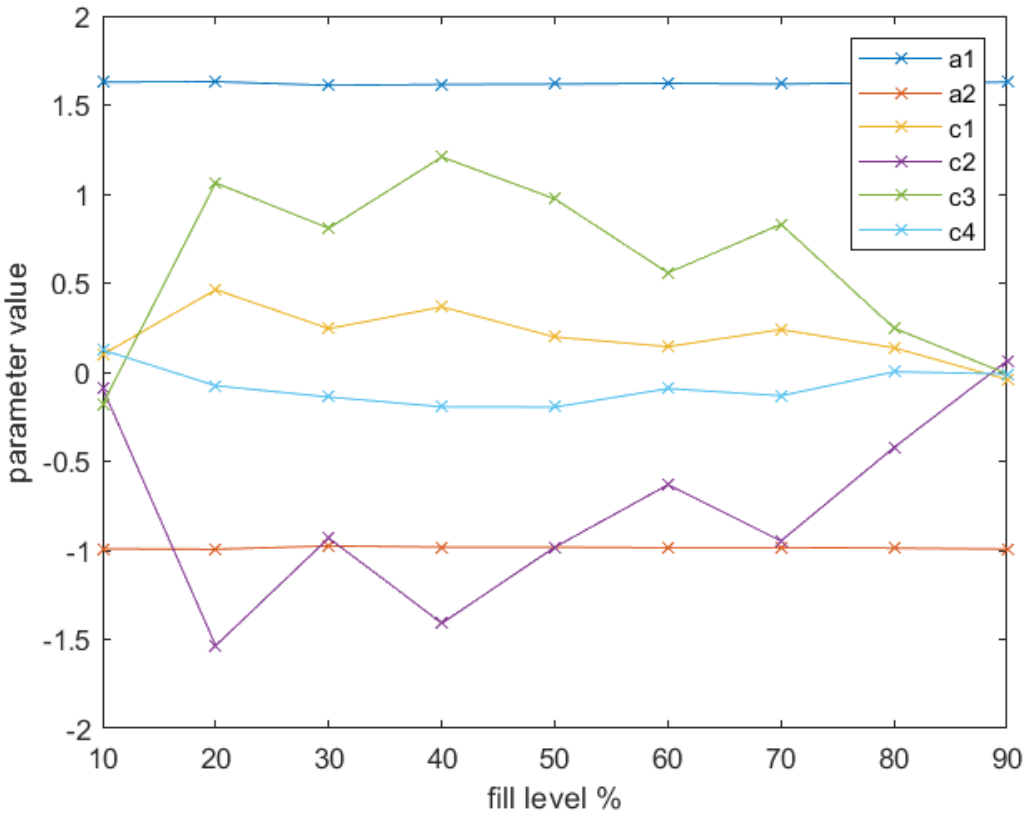

Figure 17. Estimated IV Linear and Cubic Parameters for different fill levels

5 Conclusions

Transient responses of a one DOF sloshing system have been curve-fitted using a nonlinear Autoregressive model to investigate whether it is possible to use such a continuous model rather than a piecewise linear model. This preliminary investigation has indicated that such an approach is possible and that reasonable fits are possible using linear / cubic terms. Slight improvements can be made by adding more terms but it is not clear whether there is any benefit of this. More definitive conclusions would be possible by using a nonlinear iterative curve-fit as opposed to the linear LS / IV methods used here, and also consideration of the R3 region as well. Further studies are also required to determine the contribution of each individual parameter and to get a more precise idea of the required parameters. The outcomes of this work will lead to the eventual goal of a NARMAX model that can be used to model the response of a sloshing tank on a MDOF vibration system.

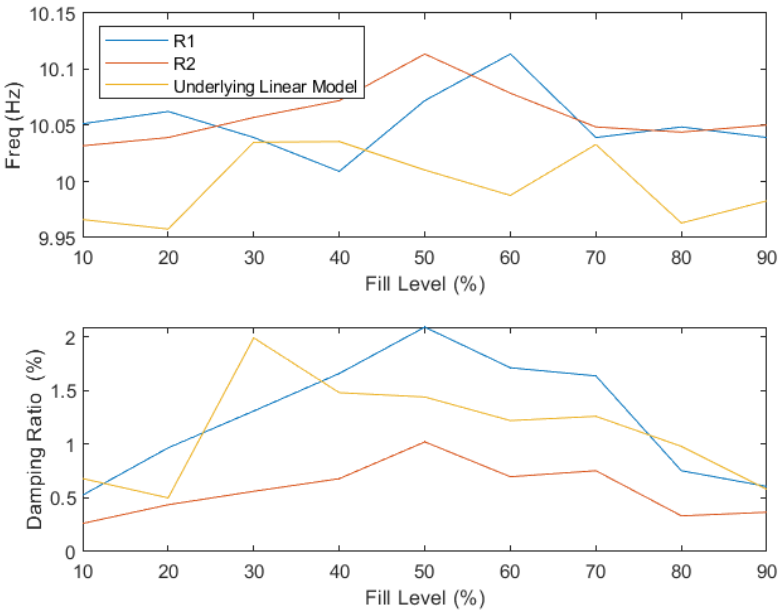

Figure 18. Frequency and Damping Estimates from R1 and R2 regions and underlying linear model

6 Acknowledgements

The research leading to this work was undertaken as part of the SLOWD project which received funding from the EU's Horizon 2020 research and innovation programme under grant agreement No. 815044.

7 References

[1] B. Titurus, J. E. Cooper, F. Saltari and e. al, "Analysis of a Sloshing Beam Experiment," *IFASD Conference*, no. 139, 2019.

[2] L. Constantin, J. deCourcy, B. Titurus, T. Rendall and J. E. Cooper, "Analysis of damping from vertical sloshing in a SDOF system.," *MSSP.*, vol. 3, no. 4, pp. 1 - 2, 2021.

[3] L. Constantin, J. deCourcy, B. Titurus, T. Rendall and J. E. Cooper, "Sloshing Induced Damping across Froude numbers in a harmonically vertically excited system.," *J Sound & Vibration*, vol. 510, 2021.

[4] J. Martinez-Carrascal, L. Constantin, M. Pizzoli and e. al, "Overview of Single Degree of Freedom Experiments of Vertical Sloshing Flows Inside Scaled Tanks," *IFASD Conference*, 2022.

[5] K. Worden and G. R. Tomlinson, "Nonlinear System Identification," *IOP*, 1987.

[6] J. E. Cooper, "Comparison of Some Time Domain System Identification Techniques using Approximate Data Correlations," *International Journal of Analytical and Experimental Modal Analysis*, vol. 4, pp. 51-57, 1989.